Biochimica et Biophysica Acta 1848 (2015) 2422–2429

Contents lists available at ScienceDirect

Biochimica et Biophysica Acta

journal homepage: www.elsevier.com/locate/bbamem

Membrane-mediated amyloid formation of PrP 106–126: A kinetic study

Yen Sun [a], Wei-Chin Hung [b], Ming-Tao Lee [c,d], Huey W. Huang [a,*]

[a] Department of Physics and Astronomy, Rice University, Houston, TX 77005, USA
[b] Department of Physics, R. O. C. Military Academy, Fengshan, Kaohsiung 83055, Taiwan
[c] National Synchrotron Radiation Research Center, Hsinchu 30076, Taiwan
[d] Department of Physics, National Central University, Jhongli 32001, Taiwan

ARTICLE INFO

Article history:
Received 15 April 2015
Received in revised form 13 July 2015
Accepted 23 July 2015
Available online 26 July 2015

Keywords:
Prion protein
Lipid extracting effect
Neurodegenerative diseases
Amyloidal peptides
Circular dichroism
Giant unilamellar vesicles

ABSTRACT

PrP 106–126 conserves the pathogenic and physicochemical properties of the Scrapie isoform of the prion protein. PrP 106–126 and other amyloidal proteins are capable of inducing ion permeability through cell membranes, and this property may represent the common primary mechanism of pathogenesis in the amyloid-related degenerative diseases. However, for many amyloidal proteins, despite numerous phenomenological observations of their interactions with membranes, it has been difficult to determine the molecular mechanisms by which the proteins cause ion permeability. One approach that has not been undertaken is the kinetic study of protein–membrane interactions. We found that the reaction time constant of the interaction between PrP 106–126 and membranes is suitable for such studies. The kinetic experiment with giant lipid vesicles showed that the membrane area first increased by peptide binding but then decreased. The membrane area decrease was coincidental with appearance of extramembranous aggregates including lipid molecules. Sometimes, the membrane area would increase again followed by another decrease. The kinetic experiment with small vesicles was monitored by circular dichroism for peptide conformation changes. The results are consistent with a molecular simulation following a simple set of well-defined rules. We deduced that at the molecular level the formation of peptide amyloids incorporated lipid molecules as part of the aggregates. Most importantly the amyloid aggregates desorbed from the lipid bilayer, consistent with the macroscopic phenomena observed with giant vesicles. Thus we conclude that the main effect of membrane-mediated amyloid formation is extraction of lipid molecules from the membrane. We discuss the likelihood of this effect on membrane ion permeability.

1. Introduction

Amyloids and their toxicity have been related to the onset and progression of amyloidoses, including neurodegenerative diseases and type II diabetes [1,2]. In each case, misfolding and aggregation of a native protein are correlated to cell death. Studies from many laboratories have suggested that the molecular agents causing amyloidoses are not the macroscopic, insoluble protein fibrils that have long been taken as the defining feature of these disorders; instead the soluble, transient, prefibrillar protein oligomers have been implicated as the primary causative agents [3–8]. While the molecular structures of the fibrillar amyloids [9–11] and the prefibrillar oligomers [8,12] are being clarified, the mechanism by which either the fibrillar or the prefibrillar species trigger cell death is still unknown. Since the early 2000's there emerged several lines of evidence pointing to a common mechanism for most or all amyloid proteins. Firstly, the cytotoxicity of a range of proteins that are able to aggregate in vitro into fibrils but are not associated with amyloid diseases suggests inherent toxicity of protein aggregates [1,13]. Secondly, all amyloid fibrils have a common atomic structure [10,11,14] and so do the prefibrillar protein oligomers [2,7,12]. Thirdly, many amyloid proteins have been found to induce ion leakage through lipid bilayers [15,16], thus if acting on cell membranes the effect could lead to loss of membrane potential and cell death. Studies [16] found that unrelated amyloidal proteins all permeabilized lipid bilayers to a similar degree and all ion-conductivities occurred without any evidence of discreet channel or pore or ion selectivity. This is consistent with independent reports of unregulated membrane permeabilization induced by many known amyloid proteins, although some of them were assumed to form pores based on pore-like AFM images (see review [2]).

There have been many studies on membrane binding by amyloid peptides and subsequent structural transformations of the peptides (see reviews [2,17,18]). In general, at very low concentrations, for example in biological fluids, the peptides remain monomeric and unstructured. However, amyloid peptides being amphipathic have relatively high affinities for membrane binding. Upon binding to lipid bilayers, the peptides transform to helical and/or β-sheet structures, depending on the peptide to lipid ratios. There are at least two different hypotheses about how amyloid peptides might affect the membrane permeability to ions. One hypothesis is that the membrane-bound amyloids include pore-like protofibrils [19–23] that allow ions to pass through (see review [2]). Another hypothesis is that amyloids cause membrane

* Corresponding author.
E-mail address: hwhuang@rice.edu (H.W. Huang).

http://dx.doi.org/10.1016/j.bbamem.2015.07.014
0005-2736/

permeability by perturbing the membrane structure, but not by pore formation [24–30]. However, most experiments were not able to show how amyloid peptides perturbed membrane structures.

Because this is such a difficult problem, we believe that it is useful to know the time sequence of peptide–membrane interactions as a function of peptide to lipid ratio. This will help clarify the molecular process of the interactions. Such kinetic studies are possible only if the time constant of interaction is compatible with the method of measurement. We found such a case in PrP 106–126.

Many notable neurodegenerative diseases in mammals such as Creutzfeldt–Jakob disease, Kuru and bovine spongiform encephalopathy are associated with an abnormal Scrapie isoform of prion protein (PrP^{Sc}) [31]. PrP 106–126, a 21-residue peptide derived from the unstructured N-terminal of the full-length prion protein, has been found to form amyloid fibrils [7,32,33] and conserve the pathogenic and physicochemical properties of PrP^{Sc} [34–36], consequently it has been used as a model peptide to study prion-related diseases. Like many other amyloid peptides, PrP 106–126 has been shown to interact with model membranes of various compositions [37], induce liposome aggregation [37,38], and form ion channels or pores in planner lipid bilayers [39,40]. On the other hand, it was also found to increase the membrane conductance without any evidence of discrete channel or pore formation or ion selectivity [16]. Miura et al. [41] studied the circular dichroism (CD) spectra of PrP 106–126 as a function of peptide-to-lipid ratio and the role of negatively charged lipids, particularly that of gangliosides in its β-sheet formation. Their results are invaluable for our design of kinetic experiments.

2. Experiment and method

2.1. Materials

1,2-Dioleoyl-*sn*-glycero-3-phosphocholine (DOPC), 1,2-dioleoyl-sn-glycero-3-phospho-(1′-rac-glycerol) (DOPG), and 1,2-dioleoyl-sn-glycero-3-phosphoethanolamine-N-(lissamine rhodamine B sulfonyl) (Rh-DOPE) were purchased from Avanti Polar Lipids (Alabaster, AL). PrP 106–126 with blocked termini (acetyl-KTNMKHMAGAAAAGAVVGGLG-amide) was synthesized by GenScript (Piscataway, NJ) and PrP 106–126 with free termini (KTNMKHMAGAAAAGAVVGGLG) was purchased from AnaSpec (Fremont, CA), both are of >95% purity. Dipotassium hydrogen phosphate (K_2HPO_4) and potassium dihydrogen phosphate (KH_2PO_4) were from Fisher Scientific (Waltham MA). All materials were used as delivered.

2.2. Kinetic experiment with SUV

To form small unilamellar vesicles (SUVs) of 7:3 DOPC and DOPG, lipids were first dissolved in chloroform to a concentration of 25 mg/ml. The solvent first evaporated under a stream of nitrogen and was further removed in a vacuum desiccator for at least 60 min. Multilamellar vesicles (MLVs) were prepared by swelling the resulted lipid film in aqueous solution to a final concentration of 10 mg/ml, then vortexing periodically for 5 min. A cup-horn sonicator was then used to sonicate the MLVs for 20 min to produces small unilamellar vesicles (SUVs). Finally, SUVs were passed through track-etched polycarbonate membranes with 30-nm pores at least 19 times using a mini-extruder apparatus (Avanti Polar Lipids, Alabaster, AL, USA). All SUVs were used on the same day of preparation.

PrP peptides at a final concentration of 100 μM were mixed with a SUV suspension in phosphate buffer (pH 6.0) at a chosen peptide-to-lipid ratio for CD measurement. CD spectra were measured in a Jasco (Tokyo, Japan) J-810 Spectropolarimeter. The spectra were scanned at room temperature in a sealed, quartz optical cell with a 1 mm path length, from wavelength 185 to 250 nm at a scan rate of ~4 min/scan. The first scan was measured right after the mixing and subsequently the sample was scanned at the time indicated in the figures below.

2.3. Kinetic experiment with aspirated GUV

The method of micropipette aspiration of giant unilamellar vesicles (GUVs) was a modification of the original method of Kwok and Evans [42] as described in Sun et al. [43,44]. A micropipette was connected to

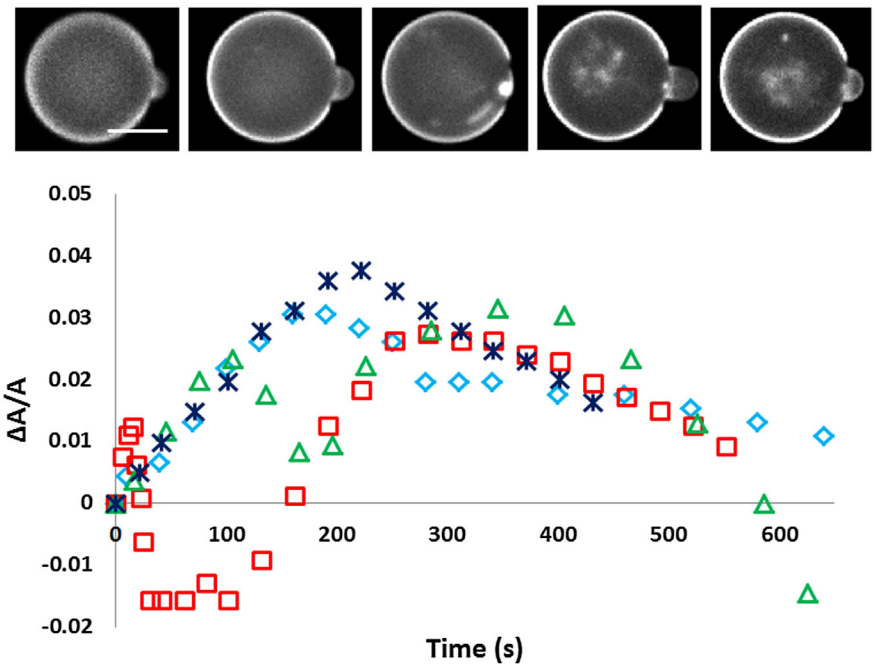

Fig. 1. Four representative runs of an aspirated GUV (containing 1% Rh-DOPE) exposed to 10 μM PrP 106–126 (out of 26 individual runs). The fractional change of the membrane area of the GUV, $\Delta A/A$, was calculated from the change of the protrusion length as shown in the fluorescence images at the top, taken at 0, 15, 95, 318, 598 s from left to right for the run labeled by red squares. Scale bar = 10 μm. Note that extramembranous aggregates containing dye lipid began to appear as the protrusion length decreased for the first time. The plot includes two representative runs showing that the membrane area increased and decreased twice in 10 min, and two other representative runs showing that the membrane area increased and decreased once in 10 min.

a water-filled U tube manometer and a negative pressure (~100 Pa producing a membrane tension ~ 0.4 mN/m) in the pipette was produced by adjusting the height of the water level reference to the atmosphere pressure [43]. An aspirated GUV consisted of a spherical part and a cylindrical part (a protrusion into the micropipette), where L_p the length of the protrusion, R_p the radius of the micropipette, and R_v the radius of the spherical part were carefully measured. Then it was straightforward to show $\Delta A = 2\pi R_p \Delta L_p + 8\pi R_v \Delta R_v$, and $\Delta V = \pi R_p^2 \Delta L_p + 4\pi R_v^2 \Delta R_v$ [42]. As long as the osmolality balance between the inside and outside of the GUV was maintained, there should be no change of the GUV volume (the effect of the pressure change by suction was so small that its contribution to the chemical potential change was ~10^{-3} that of osmolality). Under the condition $\Delta V = 0$, ΔA was directly proportional to ΔL_p: $\Delta A = 2\pi R_p(1 - R_p/R_v)\Delta L_p$. The fractional area change $\Delta A/A$ was calculated from the change of the protrusion length ΔL_p. The osmolality of every solution used in the GUV experiment was measured by a dew-point Wescor osmometer (model 5520) (Logan, UT).

There is an important limitation to the aspirated GUV experiment due to water evaporation. Water evaporation would increase the osmolality of the sample solution relative to that inside the GUV and consequently cause an increase in the protrusion length, creating errors, i.e., a background increase, in the measurement of membrane area change [43]. By humidifying the air surrounding the sample chamber, we could limit the errors of the $\Delta A/A$ measurement to a negligible level within the first several minutes, and then the background would more or less increase linearly to less than 1% within 10 min of GUV experiment [43]. Thus we limited our aspirated GUV experiments to within 10 min, and understood that the measured values of $\Delta A/A$ might include positive errors up to 1% at the end of 10 min.

3. Results

3.1. PrP peptides

We experimented with PrP 106–126 both with free termini and blocked termini. Both exhibited the same CD spectra and have the same structure transformation kinetics. We found that the GUV response to the free-termini PrP was relatively fast, therefore it was used for the GUV experiment to shorten the time of observation. The blocked PrP peptide has a slower structural transition in SUV experiments. It is more suitable for the SUV kinetic experiments. As shown by Miura et al. [41], the membrane binding affinity of PrP peptides is enhanced by lowering pH to ~6. We performed all of our experiments at pH = 6. We stress that this is only to speed up the kinetics. The results of PrP–lipid interactions are not pH-dependent as far as we know.

3.2. Macroscopic observation with GUV

GUVs of 7:3 DOPC/PG were produced in 200 mM sucrose solution [43,45]. For each run of experiment, an aspirated GUV was transferred to a chamber containing PrP peptides in a phosphate buffered (2 mM, pH 6.0) sucrose (~198 mM) solution of osmolality equal to that of the GUV content. Without PrP peptides in the solution, the GUVs showed no changes. With 50 μM blocked termini PrP peptides, we found that the GUV membrane area increased < 2% in 10 min. Free termini PrP peptides have a stronger membrane binding affinity than blocked termini PrP peptides. With free termini PrP peptides, we observed a membrane area increase ≤ 2% in 10 min for peptide concentrations ≤ 5 μM. We performed the GUV experiments with free termini PrP peptide at 10 μM.

Fig. 1 shows representative GUV responses to 10 μM free termini PrP peptide. In general, the membrane area of the GUV initially increased 3–4% within 3 min. Then the protrusion length began to decrease and extramembranous aggregates appeared. The aggregates were most clearly seen when they appeared near the equator of the GUV where the microscope's focal plane was set. In about 30% of the runs, the GUV membrane area increased and decreased twice within 10 min. This phenomenon has been previously observed in GUVs interacting with penetratin [45].

3.3. Kinetic experiment with SUV

PrP peptide was mixed with SUV (7:3 DOPC/DOPG) suspensions at different lipid concentrations from 0.35 mg/ml to 8 mg/ml. The background CD spectrum for each sample was measured without the peptide. This background was removed from each reported CD spectrum below. All samples had the same amount of peptide (100 μM) except for lipid at 8 mg/ml which was mixed with 50 μM PrP. First we

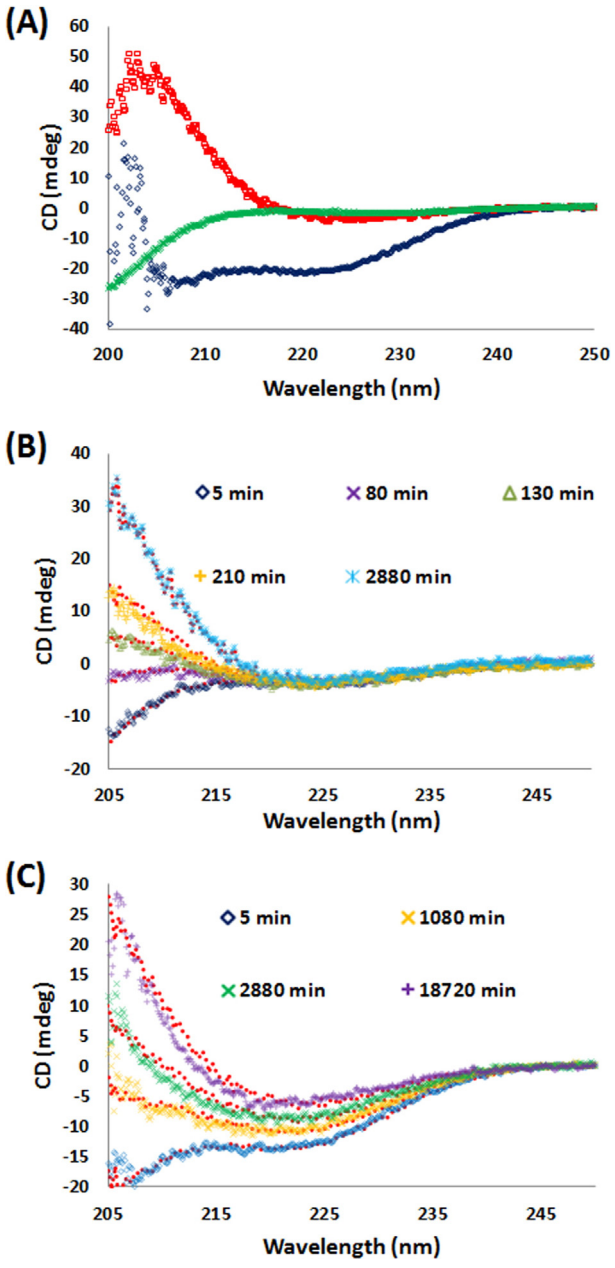

Fig. 2. (A) CD spectra of PrP 106–126 in three different configurations: α-helix (blue), β-sheet (red), and random coil (green) in a unit expressed in mdeg for the same concentration of 100 μM of peptide. (B) Time series of CD spectra, from bottom to top, for 100 μM PrP peptide in 0.7 mg/ml lipid vesicles ($P_t/L = 1/9$). (C) Time series of CD spectra, from bottom to top, for 100 μM PrP peptide in 4 mg/ml lipid vesicles ($P_t/L = 1/50$). In both (B) and (C), the data are shown by the symbols indicated by the time of measurement, and the red dots are the fit to a linear combination of three spectra shown in (A). All measurements were made with the same amount of peptide, so all CD spectra are normalized relatively to each other.

established the CD spectra of PrP peptide in three configurations (Fig. 2A). In a pure phosphate buffer, the peptide was in a random coil configuration; in 4 mg/ml SUV of 1:1 DOPC/DOPG suspension the peptide had a CD of the α-helical configuration, closely similar to its CD in tetrafluoroethylene; in 2 mg/ml suspension the peptide evolved to a stable β-sheet configuration after one day (Fig. 2A).

Each kinetic experiment started with PrP peptides in the monomeric random-coil state. Lipid vesicles of DOPC/DOPG 7:3 at various total peptide to lipid ratios (P_t/L) were mixed with the peptide. The first CD measurement of a sample completed in about 4 min (shown as t = 0 in Figs. 3 and 4). Subsequently, depending on the rate of change, CD was measured at longer time intervals. As examples, two series of kinetic measurements are shown in Fig. 2B and C. Each CD spectrum was decomposed into the components of random-coil, α-helical and β-sheet states by linear fitting. The kinetic data are presented in Fig. 3 for large P_t/L values and in Fig. 4 for small P_t/L values. The SUVs in the samples reported in Figs. 3 and 4 did not cause significant light scattering. However samples of any lower P_t/L value (higher lipid concentrations) would have significant light scattering that distorts the CD spectra.

4. Discussion

Amyloid aggregation of proteins in solution has been described as nucleation-dependent polymerization [1,46]. It has been argued that this is a general property of polypeptides [13,47], but at physiological concentrations polymerization is normally prevented from occurring by the energy barrier for nucleation [1]. Here we take the view that the toxicity of the amyloid peptide occurs if the amyloid formation process is mediated by cell membranes, since membrane permeabilization to ions has been repeatedly detected in the presence of amyloidal peptides (see refs cited in [2,16]). Indeed, membranes have been implicated as the catalyst that facilities amyloid formation (see review [17,48,49]). For many peptides, such as Aβ [17,50], IAPP [18,29,51], PrP [41], and penetratin [45,52] it has been known that unstructured peptide monomers in solution transform into α-helices upon binding to membranes. As the bound peptide to lipid ratio, P_b/L, increases, peptides were found in β-sheets, presumably in an aggregated form. Is there an energy barrier for the membrane-mediated β-sheet formation? What is the effect of this transformation to the membrane

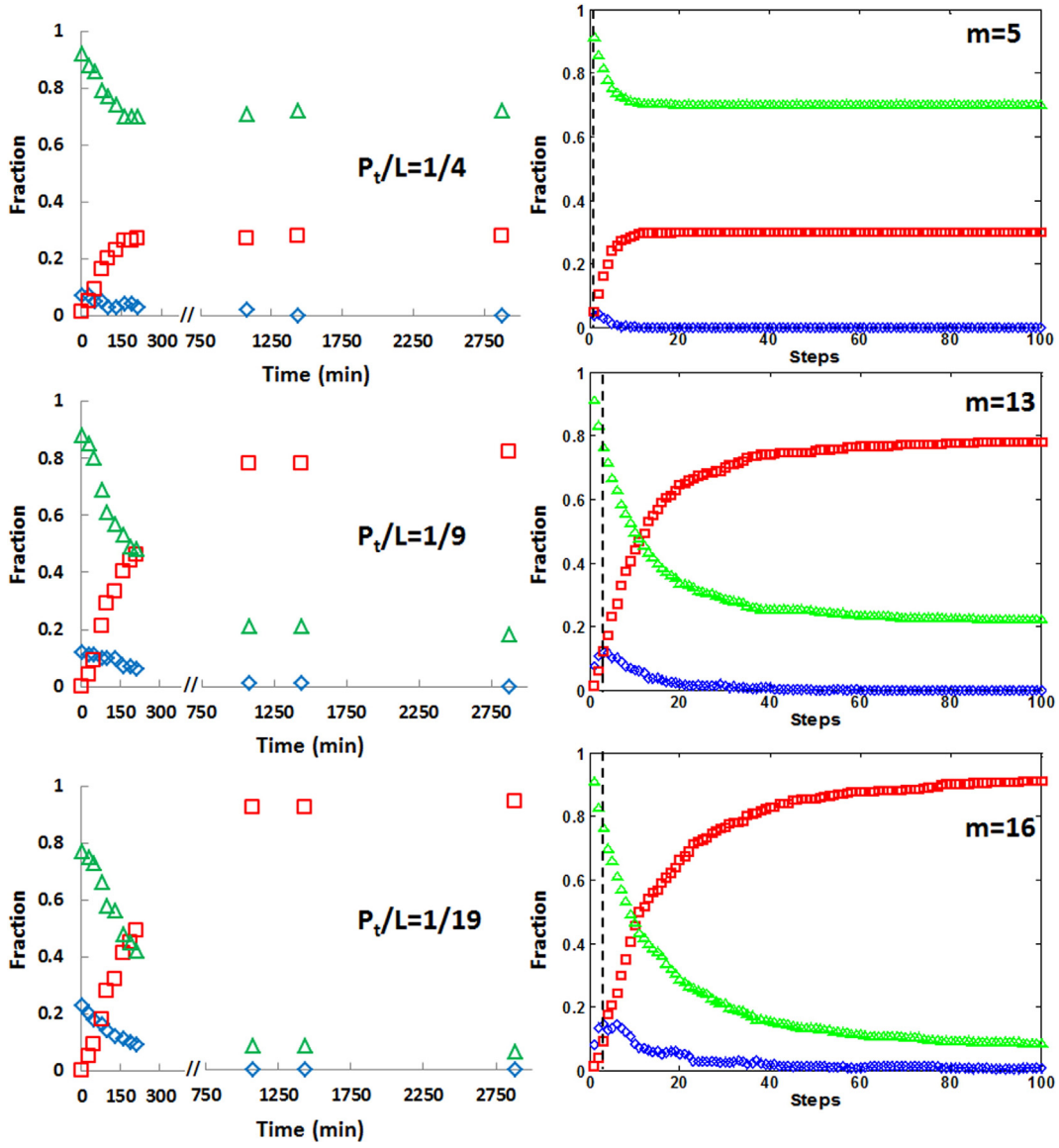

Fig. 3. Kinetics of PrP peptide conformation changes at high total peptide to lipid ratios (P_t/L). The sample conditions were: 100 μM PrP in 0.35 mg/ml lipid ($P_t/L = 1/4$), in 0.7 mg/ml lipid ($P_t/L = 1/9$), and in 1.5 mg/ml lipid ($P_t/L = 1/19$). Data are on the left column (note the initial time scale expansion), and the corresponding simulations on the right, where m is the number of lipid vesicles in simulations (see text or the Supporting information). Each simulation result was the average of five repeated simulations. Green represents the fraction of the peptide in random coils, blue α-helices and red β-sheets. The black dashed lines in simulations are the "starting time" to be compared with the first measurements in the kinetic experiments.

properties? These are important questions, if the amyloid formation in membranes is indeed the cause of toxicity.

We suspect that amyloid formation might affect the membrane properties because we have observed in GUV experiments that amyloid peptides, such as hIAPP [29] and penetratin [45,52], formed extramembranous aggregates including lipids that desorbed from the lipid bilayers of the vesicles. The appearance of the extramembranous aggregates was coincidental with the decrease of membrane area, consistent with the membrane losing lipid molecules [29,45,52]. These were macroscopic observations. The aggregates caused by amyloid peptides must grow to a micron or larger scale to be seen under microscope. The time constant for forming macroscopic aggregates varies with peptides: relatively short for penetratin [45,52], longer for hIAPP [29]. If lipid vesicles were suspended in solution with amyloid peptides, eventually very large aggregates including lipids would appear [29,53]. The effect of the PrP peptide on GUVs (Fig. 1) is the same as penetratin and hIAPP. First the binding of PrP peptide to a GUV caused a membrane area expansion implying that the peptides inserted into the headgroup region of the bilayer (this was called a wedge effect [54,55]). Then the expansion stopped and the area began to decrease indicating that the lipid bilayer was losing peptide or lipid or both. Within the experimental time limit of ~10 min (see Experiment and method), sometimes the GUV membrane area would increase and decrease twice. Large extramembranous aggregates including lipid molecules were occasionally visible during the membrane area decrease. If lipid vesicles were suspended in a solution containing PrP 106–126, networks of aggregates, characteristic of amyloid aggregation including lipids [29,53], inevitably appeared (Fig. 5). [Note that the time scale for aggregation is much shorter in a GUV experiment (Fig. 1) than in a SUV suspension (Figs. 3, 4, 5), because the peptide to lipid ratio is many orders of magnitude higher in the former than in the latter [56].] The GUV experiments offered a large scale observation of the lipid extracting effect. To see if the same effect is extended to the molecular level, we performed kinetic experiments with SUVs where we monitored the peptide conformation transformation and interpreted the data with a simple molecular simulation.

In the kinetic experiment with SUVs, the first CD scan completed ~ 4 min after mixing was always a linear combination of

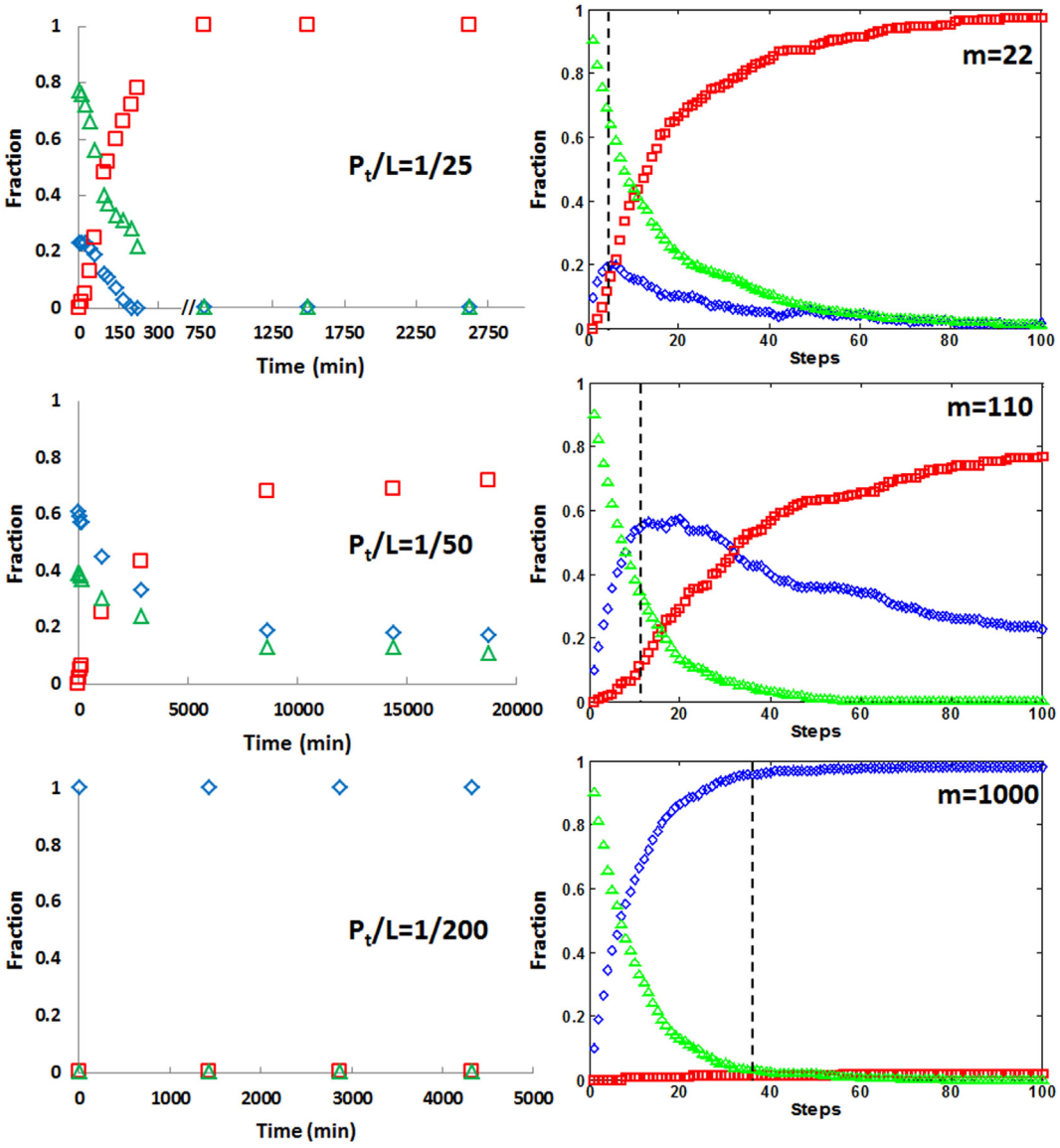

Fig. 4. Kinetics of PrP peptide conformation changes at low total peptide to lipid ratios (P_t/L). The sample conditions were: 100 μM PrP in 2 mg/ml lipid ($P_t/L = 1/25$), and in 4 mg/ml lipid ($P_t/L = 1/50$); 50 μM PrP in 8 mg/ml lipid ($P_t/L = 1/200$). Data are on the left column (note the initial time scale expansion for $P_t/L = 1/25$), and the corresponding simulations on the right, where m is the number of lipid vesicles in simulations (see text or the Supporting information). Each simulation result was the average of five repeated simulations. Green represents the fraction of the peptide in random coils, blue α-helices and red β-sheets. The black dashed lines in simulations are the "starting time" to be compared with the first measurements in the kinetic experiments.

random coils and alpha helices, and the helical component increased with increasing lipid concentration. The kinetics of peptide binding to lipid vesicles was too fast to be detected by CD measurement. (We measured the spectral intensity change at one wavelength of 201.5 nm immediately after mixing and found that the change was completed within 20 s—see Supporting information Fig. S1.) As time went on, both the α-helical and random coil components decreased while the β-sheet component increased (Figs. 3 and 4). We used a set of simple rules to numerically simulate these data (see details in the Supporting information). A simulation starts with 100 peptide monomers and m number of vesicles, each of which has 12 lipid-sites for peptide binding. Each Monte Carlo (MC) step picks a peptide: (i) If the peptide is random-coil, it probabilistically binds to an empty lipid-site and transforms to a helix, otherwise remains a random-coil. If the peptide finds a binding site in a vesicle, and if the number of helices in the vesicle is less than a critical P_b/L^* value of 1/4, the helices in this vesicle stay. But if the number of helices in the vesicle reaches a P_b/L value of 1/4, all of the peptides in that vesicle transform to a β-aggregate and simultaneously the vesicle loses 4 lipid-sites as part of the aggregate. After the desorption of the peptide–lipid aggregate, the vesicle becomes smaller and continues to bind peptides. (ii) If the MC step picks a helical peptide, the helix is allowed to transfer to another empty lipid-site, presumably through vesicle–vesicle collision. Again the rule of transformation to a β-aggregate applies after the transfer. (iii) If the MC step picks a β-sheet peptide, nothing changes. The actual program is given in the Supporting information. The simulation results are compared with the kinetic data in Figs. 3 and 4.

By making the MC steps corresponding to the experimental time, we note that in the experiment all peptides react with membranes simultaneously, while a simulation takes only one peptide molecule in each step. Therefore the "time" has been stretched out in simulations. Since the binding of peptides to vesicles was too fast to be measured by CD, in each simulation (Figs. 3 and 4), we drew a "starting time" (the dashed lines in Figs. 3 and 4) corresponding to the time of the first measurement. We also note that in the experiment there is a time delay in converting α-helices to β-aggregates—note that the β-sheet component was zero at the first CD measurement in each case which was completed in ~4 min while the initial peptide binding was completed within 20 s. This suggests that there might be a nucleation barrier for membrane-bound helical peptides converting to β-sheet aggregates. Thus our "starting time" in simulation was the time the α-helix component reached the maximum, because in the experiment this was when β-sheets began to form. This "starting time" took more MC steps as the ratio P_b/L decreased, because more peptides were initially bound to the vesicles.

Once we take into account the MC "time," we see an excellent qualitative agreement between the kinetic data and the simulations following the simple rules described above for a wide range of peptide to lipid ratios. Thus we are able to draw the following conclusions: (1) The peptides must bind to a membrane and turns into an α-helix before converting into a β-sheet. It is very well known that the amyloid peptides appear as helices at low P_b/L, but as β-sheets at high P_b/L. However, only the kinetic experiments show that β-sheets come from helices, not directly from random coils. (2) The membrane bound helices must reach a critical value of P_b/L^* before converting into β-sheets. In the $P_t/L = 1/200$ case, all peptides remained in the α-helical state; there were no β-sheets, because P_b/L was below the critical value. (3) The GUV experiments showed large PrP peptide aggregates desorbed from the lipid bilayer, same as in previous GUV experiments with other amyloid peptides [29,45,52,57]—we called this a lipid extracting effect because lipid molecules were part of the extramembranous aggregates. Accordingly in simulations we assumed that the lipid vesicles lost lipid molecules whenever β-sheet aggregates were formed. (4) After losing lipid molecules to extramembranous aggregates, the vesicle membrane continued to bind peptides as demonstrated in the GUV experiment (Fig. 1). We wish to draw attention to the kinetic results, particularly obvious in Fig. 3, that the amount of final β-sheet component was much higher than the maximum α-helical component from the initial binding, which completed within ~20 s. Thus a substantial amount of the final β-sheet component had to come from the peptides subsequently bound to lipid vesicles after

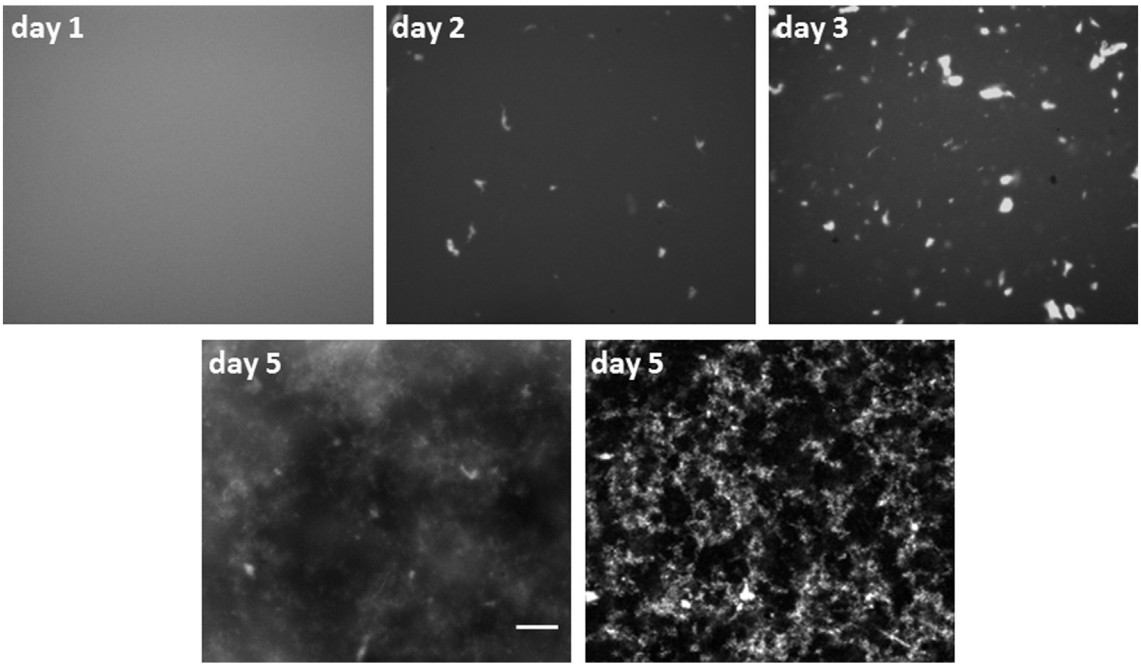

Fig. 5. The fluorescence images of 100 μM PrP peptide mixed with 0.5 mg/ml lipid vesicles made of 7:3 DOPC/DOPG and 1% of Rh-DOPE ($P_t/L = 1/9$), at the time indicated. Initially the aggregates were too small to be detected, but the aggregates grew to macroscopic size as time went on. An additional confocal image was shown for day 5. These images show that the lipid was part of the aggregates formed by PrP peptides. Scale bar = 50 μm.

the peptides from the initial binding had converted to β-aggregates and desorbed from the lipid vesicles. In the high P_t/L cases (e.g., $P_t/L = 1/4$ and $P_t/L = 1/9$), the lipid molecules were eventually used up—all became part of the β-sheet aggregates, and the excessive peptides that had not bound to vesicles remained in the random coil state.

Thus we conclude that the main perturbation effect the amyloid peptides exert on membranes is extracting lipid molecules from the membrane via the process of membrane-mediated amyloid formation. Otherwise the process left the GUV intact. This kinetic study offers a model of peptide–membrane interaction for the lipid extracting effect. Can this effect cause the membrane permeable to ions?

5. Lipid extraction and ion leakage

Ion permeation through a membrane has been extensively studied by molecular simulations [58–62]. The consensual results can be summarized as follows: (i) ion permeation is an activated process; spontaneous ion permeation is rare [61,62]; (ii) ions enter the bilayer with a trail of water molecules called water fingers [58] (the potential energy for an isolated ion in membrane is too high). The water finger is lined by lipid headgroups. This results in a major rearrangement of neighboring lipids, commonly called water pore defects [58–62]; (iii) simulations by displacing a pair of chain-to-chain lipid molecules from a bilayer create a water pore defect, allowing ion permeation [60]; and (iv) the transient water pores created by activated ion permeation or by the lipid molecule displacement have radii less than 1 nm [59], and life time of 10–100 ns [59,60]. Thus it is reasonable to expect that lipid extraction from a membrane can lead to ion permeability.

Currently there are several different suggestions about how amyloid formation might cause ion permeabilization in membranes. It has been suggested that amyloid formation includes pore-like structures within the membrane [19–23] (see review [2]); amyloid formation creates defects in membrane structures [26,27,30]; or the process of amyloid formation extracts lipid molecules and damages the membrane [24, 53]. Here we showed that the lipid extracting effect by amyloid peptides previously observed at the macroscopic scale in GUVs is consistent at the molecular scale by kinetic experiments with SUVs. We showed that membrane-mediated amyloid formation is a cooperative transition by membrane-bound α-helices to β-aggregates which occurs only when P_b/L exceeds a critical value. The β-aggregates desorb from the membrane, but otherwise leave the GUV intact. The desorbed aggregates include lipid molecules, implying lipid extraction from the membrane. Therefore we propose that the process of lipid extraction creates transient water defects in the membrane resulting in ion permeability.

Transparency Document

The Transparency document associated with this article can be found, in the online version.

Acknowledgments

This work was supported by NIH (US) Grant GM55203, the Robert A. Welch Foundation Grant C-0991 (H.W.H.); and by Taiwan MOST 103-2112-M-216-003 (W.C.H. and M.T.L.).

Appendix A. Supplementary data

Supplementary data to this article can be found online at http://dx.doi.org/10.1016/j.bbamem.2015.07.014.

References

[1] M.F. Perutz, A.H. Windle, Cause of neural death in neurodegenerative diseases attributable to expansion of glutamine repeats, Nature 412 (2001) 143–144.
[2] H.A. Lashuel, P.T. Lansbury Jr., Are amyloid diseases caused by protein aggregates that mimic bacterial pore-forming toxins? Q. Rev. Biophys. 39 (2006) 167–201.
[3] B. Caughey, P.T. Lansbury, Protofibrils, pores, fibrils, and neurodegeneration: separating the responsible protein aggregates from the innocent bystanders, Annu. Rev. Neurosci. 26 (2003) 267–298.
[4] W.F. Xue, A.L. Hellewell, W.S. Gosal, S.W. Homans, E.W. Hewitt, S.E. Radford, Fibril fragmentation enhances amyloid cytotoxicity, J. Biol. Chem. 284 (2009) 34272–34282.
[5] R. Kodali, R. Wetzel, Polymorphism in the intermediates and products of amyloid assembly, Curr. Opin. Struct. Biol. 17 (2007) 48–57.
[6] M.D. Kirkitadze, G. Bitan, D.B. Teplow, Paradigm shifts in Alzheimer's disease and other neurodegenerative disorders: the emerging role of oligomeric assemblies, J. Neurosci. Res. 69 (2002) 567–577.
[7] R. Kayed, E. Head, J.L. Thompson, T.M. McIntire, S.C. Milton, C.W. Cotman, C.G. Glabe, Common structure of soluble amyloid oligomers implies common mechanism of pathogenesis, Science 300 (2003) 486–489.
[8] C.G. Glabe, Structural classification of toxic amyloid oligomers, J. Biol. Chem. 283 (2008) 29639–29643.
[9] O. Sumner Makin, L.C. Serpell, Structural characterisation of islet amyloid polypeptide fibrils, J. Mol. Biol. 335 (2004) 1279–1288.
[10] M. Balbirnie, R. Grothe, D.S. Eisenberg, An amyloid-forming peptide from the yeast prion Sup35 reveals a dehydrated beta-sheet structure for amyloid, Proc. Natl. Acad. Sci. U. S. A. 98 (2001) 2375–2380.
[11] R. Nelson, M.R. Sawaya, M. Balbirnie, A.O. Madsen, C. Riekel, R. Grothe, D. Eisenberg, Structure of the cross-beta spine of amyloid-like fibrils, Nature 435 (2005) 773–778.
[12] A. Laganowsky, C. Liu, M.R. Sawaya, J.P. Whitelegge, J. Park, M. Zhao, A. Pensalfini, A.B. Soriaga, M. Landau, P.K. Teng, D. Cascio, C. Glabe, D. Eisenberg, Atomic view of a toxic amyloid small oligomer, Science 335 (2012) 1228–1231.
[13] M. Bucciantini, E. Giannoni, F. Chiti, F. Baroni, L. Formigli, J. Zurdo, N. Taddei, G. Ramponi, C.M. Dobson, M. Stefani, Inherent toxicity of aggregates implies a common mechanism for protein misfolding diseases, Nature 416 (2002) 507–511.
[14] R. Nelson, D. Eisenberg, Structural models of amyloid-like fibrils, Adv. Protein Chem. 73 (2006) 235–282.
[15] M. Anguiano, R.J. Nowak, P.T. Lansbury Jr., Protofibrillar islet amyloid polypeptide permeabilizes synthetic vesicles by a pore-like mechanism that may be relevant to type II diabetes, Biochemistry 41 (2002) 11338–11343.
[16] R. Kayed, Y. Sokolov, B. Edmonds, T.M. McIntire, S.C. Milton, J.E. Hall, C.G. Glabe, Permeabilization of lipid bilayers is a common conformation-dependent activity of soluble amyloid oligomers in protein misfolding diseases, J. Biol. Chem. 279 (2004) 46363–46366.
[17] K. Matsuzaki, Physicochemical interactions of amyloid beta-peptide with lipid bilayers, Biochim. Biophys. Acta 1768 (2007) 1935–1942.
[18] J.R. Brender, S. Salamekh, A. Ramamoorthy, Membrane disruption and early events in the aggregation of the diabetes related peptide IAPP from a molecular perspective, Acc. Chem. Res. 45 (2012) 454–462.
[19] J.H. Hafner, C.L. Cheung, A.T. Woolley, C.M. Lieber, Structural and functional imaging with carbon nanotube AFM probes, Prog. Biophys. Mol. Biol. 77 (2001) 73–110.
[20] H. Lin, R. Bhatia, R. Lal, Amyloid beta protein forms ion channels: implications for Alzheimer's disease pathophysiology, FASEB J. 15 (2001) 2433–2444.
[21] F. Sokolowski, A.J. Modler, R. Masuch, D. Zirwer, M. Baier, G. Lutsch, D.A. Moss, K. Gast, D. Naumann, Formation of critical oligomers is a key event during conformational transition of recombinant Syrian hamster prion protein, J. Biol. Chem. 278 (2003) 40481–40492.
[22] T.A. Mirzabekov, M.C. Lin, B.L. Kagan, Pore formation by the cytotoxic islet amyloid peptide amylin, J. Biol. Chem. 271 (1996) 1988–1992.
[23] J. Janson, R.H. Ashley, D. Harrison, S. McIntyre, P.C. Butler, The mechanism of islet amyloid polypeptide toxicity is membrane disruption by intermediate-sized toxic amyloid particles, Diabetes 48 (1999) 491–498.
[24] E. Sparr, M.F. Engel, D.V. Sakharov, M. Sprong, J. Jacobs, B. de Kruijff, J.W. Hoppener, J.A. Killian, Islet amyloid polypeptide-induced membrane leakage involves uptake of lipids by forming amyloid fibers, FEBS Lett. 577 (2004) 117–120.
[25] J.D. Green, C. Goldsbury, J. Kistler, G.J. Cooper, U. Aebi, Human amylin oligomer growth and fibril elongation define two distinct phases in amyloid formation, J. Biol. Chem. 279 (2004) 12206–12212.
[26] T.A. Harroun, J.P. Bradshaw, R.H. Ashley, Inhibitors can arrest the membrane activity of human islet amyloid polypeptide independently of amyloid formation, FEBS Lett. 507 (2001) 200–204.
[27] H. Zhao, E.K. Tuominen, P.K. Kinnunen, Formation of amyloid fibers triggered by phosphatidylserine-containing membranes, Biochemistry 43 (2004) 10302–10307.
[28] P. Walsh, G. Vanderlee, J. Yau, J. Campeau, V.L. Sim, C.M. Yip, S. Sharpe, The mechanism of membrane disruption by cytotoxic amyloid oligomers formed by prion protein(106–126) is dependent on bilayer composition, J. Biol. Chem. 289 (2014) 10419–10430.
[29] C.C. Lee, Y. Sun, H.W. Huang, How type II diabetes-related islet amyloid polypeptide damages lipid bilayers, Biophys. J. 102 (2012) 1059–1068.
[30] J.D. Green, L. Kreplak, C. Goldsbury, X. Li Blatter, M. Stolz, G.S. Cooper, A. Seelig, J. Kistler, U. Aebi, Atomic force microscopy reveals defects within mica supported lipid bilayers induced by the amyloidogenic human amylin peptide, J. Mol. Biol. 342 (2004) 877–887.
[31] N.R. Deleault, B.T. Harris, J.R. Rees, S. Supattapone, Formation of native prions from minimal components in vitro, Proc. Natl. Acad. Sci. U. S. A. 104 (2007) 9741–9746.
[32] M. Salmona, P. Malesani, L. De Gioia, S. Gorla, M. Bruschi, A. Molinari, F. Della Vedova, B. Pedrotti, M.A. Marrari, T. Awan, O. Bugiani, G. Forloni, F. Tagliavini, Molecular determinants of the physicochemical properties of a critical prion protein region comprising residues 106–126, Biochem. J. 342 (Pt 1) (1999) 207–214.
[33] C. Selvaggini, L. De Gioia, L. Cantu, E. Ghibaudi, L. Diomede, F. Passerini, G. Forloni, O. Bugiani, F. Tagliavini, M. Salmona, Molecular characteristics of a protease-resistant,

amyloidogenic and neurotoxic peptide homologous to residues 106–126 of the prion protein, Biochem. Biophys. Res. Commun. 194 (1993) 1380–1386.
[34] G. Forloni, N. Angeretti, R. Chiesa, E. Monzani, M. Salmona, O. Bugiani, F. Tagliavini, Neurotoxicity of a prion protein fragment, Nature 362 (1993) 543–546.
[35] T. Florio, M. Grimaldi, A. Scorziello, M. Salmona, O. Bugiani, F. Tagliavini, G. Forloni, G. Schettini, Intracellular calcium rise through L-type calcium channels, as molecular mechanism for prion protein fragment 106–126-induced astroglial proliferation, Biochem. Biophys. Res. Commun. 228 (1996) 397–405.
[36] T. Florio, S. Thellung, C. Amico, M. Robello, M. Salmona, O. Bugiani, F. Tagliavini, G. Forloni, G. Schettini, Prion protein fragment 106–126 induces apoptotic cell death and impairment of L-type voltage-sensitive calcium channel activity in the GH3 cell line, J. Neurosci. Res. 54 (1998) 341–352.
[37] B. Kurganov, M. Doh, N. Arispe, Aggregation of liposomes induced by the toxic peptides Alzheimer's Abetas, human amylin and prion (106–126): facilitation by membrane-bound GM1 ganglioside, Peptides 25 (2004) 217–232.
[38] D.L. Rymer, T.A. Good, The role of prion peptide structure and aggregation in toxicity and membrane binding, J. Neurochem. 75 (2000) 2536–2545.
[39] J.I. Kourie, P.V. Farrelly, C.L. Henry, Channel activity of deamidated isoforms of prion protein fragment 106–126 in planar lipid bilayers, J. Neurosci. Res. 66 (2001) 214–220.
[40] M.C. Lin, T. Mirzabekov, B.L. Kagan, Channel formation by a neurotoxic prion protein fragment, J. Biol. Chem. 272 (1997) 44–47.
[41] T. Miura, M. Yoda, N. Takaku, T. Hirose, H. Takeuchi, Clustered negative charges on the lipid membrane surface induce beta-sheet formation of prion protein fragment 106–126, Biochemistry 46 (2007) 11589–11597.
[42] R. Kwok, E. Evans, Thermoelasticity of large lecithin bilayer vesicles, Biophys. J. 35 (1981) 637–652.
[43] Y. Sun, W.C. Hung, F.Y. Chen, C.C. Lee, H.W. Huang, Interaction of tea catechin (−)-epigallocatechin gallate with lipid bilayers, Biophys. J. 96 (2009) 1026–1035.
[44] Y. Sun, C.C. Lee, H.W. Huang, Adhesion and merging of lipid bilayers: a method for measuring the free energy of adhesion and hemifusion, Biophys. J. 100 (2011) 987–995.
[45] Y. Sun, C.C. Lee, T.H. Chen, H.W. Huang, Kinetic process of beta-amyloid formation via membrane binding, Biophys. J. 99 (2010) 544–552.
[46] J.T. Jarrett, P.T. Lansbury Jr., Seeding “one-dimensional crystallization” of amyloid: a pathogenic mechanism in Alzheimer's disease and scrapie? Cell 73 (1993) 1055–1058.
[47] C.M. Dobson, The structural basis of protein folding and its links with human disease, Philos. Trans. R. Soc. Lond. B Biol. Sci. 356 (2001) 133–145.
[48] G.P. Gorbenko, P.K. Kinnunen, The role of lipid–protein interactions in amyloid-type protein fibril formation, Chem. Phys. Lipids 141 (2006) 72–82.
[49] S.A. Jayasinghe, R. Langen, Membrane interaction of islet amyloid polypeptide, Biochim. Biophys. Acta 1768 (2007) 2002–2009.
[50] E. Terzi, G. Holzemann, J. Seelig, Interaction of Alzheimer beta-amyloid peptide(1–40) with lipid membranes, Biochemistry 36 (1997) 14845–14852.
[51] S.A. Jayasinghe, R. Langen, Lipid membranes modulate the structure of islet amyloid polypeptide, Biochemistry 44 (2005) 12113–12119.
[52] C.C. Lee, Y. Sun, H.W. Huang, Membrane-mediated peptide conformation change from alpha-monomers to beta-aggregates, Biophys. J. 98 (2010) 2236–2245.
[53] M.F. Engel, L. Khemtemourian, C.C. Kleijer, H.J. Meeldijk, J. Jacobs, A.J. Verkleij, B. de Kruijff, J.A. Killian, J.W. Hoppener, Membrane damage by human islet amyloid polypeptide through fibril growth at the membrane, Proc. Natl. Acad. Sci. U. S. A. 105 (2008) 6033–6038.
[54] T.C. Terwilliger, L. Weissman, D. Eisenberg, The structure of melittin in the form I crystals and its implication for melittin's lytic and surface activities, Biophys. J. 37 (1982) 353–361.
[55] S. Ludtke, K. He, H. Huang, Membrane thinning caused by magainin 2, Biochemistry 34 (1995) 16764–16769.
[56] Y. Tamba, M. Yamazaki, Single giant unilamellar vesicle method reveals effect of antimicrobial peptide magainin 2 on membrane permeability, Biochemistry 44 (2005) 15823–15833.
[57] Y.F. Chen, T.L. Sun, Y. Sun, H.W. Huang, Interaction of daptomycin with lipid bilayers: a lipid extracting effect, Biochemistry 53 (2014) 5384–5392.
[58] I. Benjamin, Mechanism and dynamics of ion transfer across a liquid–liquid interface, Science 261 (1993) 1558–1560.
[59] A.A. Gurtovenko, I. Vattulainen, Ion leakage through transient water pores in protein-free lipid membranes driven by transmembrane ionic charge imbalance, Biophys. J. 92 (2007) 1878–1890.
[60] D.P. Tieleman, S.J. Marrink, Lipids out of equilibrium: energetics of desorption and pore mediated flip-flop, J. Am. Chem. Soc. 128 (2006) 12462–12467.
[61] H.L. Tepper, G.A. Voth, Mechanisms of passive ion permeation through lipid bilayers: insights from simulations, J. Phys. Chem. B 110 (2006) 21327–21337.
[62] I.V. Khavrutskii, A.A. Gorfe, B. Lu, J.A. McCammon, Free energy for the permeation of Na(+) and Cl(−) ions and their ion-pair through a zwitterionic dimyristoyl phosphatidylcholine lipid bilayer by umbrella integration with harmonic fourier beads, J. Am. Chem. Soc. 131 (2009) 1706–1716.